LETTER

doi:10.1038/nature18291

Early Neanderthal constructions deep in Bruniquel Cave in southwestern France

Jacques Jaubert[1]*, Sophie Verheyden[2,3]*, Dominique Genty[4]*, Michel Soulier[5], Hai Cheng[6,7], Dominique Blamart[4], Christian Burlet[2], Hubert Camus[8], Serge Delaby[9], Damien Deldicque[10], R. Lawrence Edwards[7], Catherine Ferrier[1], François Lacrampe-Cuyaubère[11,12], François Lévêque[13], Frédéric Maksud[14], Pascal Mora[15], Xavier Muth[12], Édouard Régnier[4], Jean-Noël Rouzaud[10] & Frédéric Santos[1]

Very little is known about Neanderthal cultures[1], particularly early ones. Other than lithic implements and exceptional bone tools[2], very few artefacts have been preserved. While those that do remain include red and black pigments[3] and burial sites[4], these indications of modernity are extremely sparse and few have been precisely dated, thus greatly limiting our knowledge of these predecessors of modern humans[5]. Here we report the dating of annular constructions made of broken stalagmites found deep in Bruniquel Cave in southwest France. The regular geometry of the stalagmite circles, the arrangement of broken stalagmites and several traces of fire demonstrate the anthropogenic origin of these constructions. Uranium-series dating of stalagmite regrowths on the structures and on burnt bone, combined with the dating of stalagmite tips in the structures, give a reliable and replicated age of 176.5 thousand years (±2.1 thousand years), making these edifices among the oldest known well-dated constructions made by humans. Their presence at 336 metres from the entrance of the cave indicates that humans from this period had already mastered the underground environment, which can be considered a major step in human modernity.

Since its natural closing during the Pleistocene period and until its discovery[6] in 1990, no humans entered Bruniquel Cave, located in southwest France (44° 4′ N, 1° 41′ E, Extended Data Fig. 1a), an area already rich in Palaeolithic sites (Extended Data Fig. 1b). Local cavers then dug through the collapsed entrance, a 30-m long and narrow passage through which persons can reach the main gallery. The structures (Fig. 1 and Extended Data Fig. 2a) are located at 336 m from the entrance after an easy walk through speleothem-rich chambers (Extended Data Fig. 1c). Near the entrance, the remains of large Pleistocene fauna and Holocene micro-fauna were found[7], and bears also left numerous traces of their presence: hibernation hollows, claw marks and a few footprints. The most notable features, however, are the strange arrangement of two annular structures made of whole and broken stalagmites (Fig. 1 and Supplementary Video 1), accompanied by numerous traces of fire (Fig. 1 and Extended Data Fig. 3). Other than these structures, signs of human activity are almost non-existent and uncertain: a stalagmite tip that seems to have been hollowed out, negative prints left by wrenching stalagmites from the ground, and a few speleothem pieces in locations other than their original ones. At present, no marks on the cave walls or footprints have been observed. A first study in the early 1990s provided a detailed plan of the structures and a single ^{14}C accelerator mass spectrometry dating of a burnt bone found in the main structure, giving an intriguing age of >47.6 thousand years ago (ka; ref. 6).

The question was whether these unique constructions were made by Neanderthals.[8,9] Unfortunately, the premature death of the archaeologist F. Rouzaud, along with the restricted access to the cave, prevented any further research until 2013 when we decided to date and study these enigmatic constructions.

The arranged structures composed of whole and broken stalagmites, here designated as 'speleofacts' (Extended Data Table 1), are located in the largest chamber of the cave (Extended Data Fig. 1c). Our study defines two categories of structures: two annular ones, which are the most impressive, and four smaller stalagmite accumulation structures (Supplementary Video 1). The largest annular structure is 6.7 × 4.5 m, and the smaller one is 2.2 × 2.1 m. The accumulation structures consist of stacks of stalagmites and are from 0.55 m to 2.60 m in diameter. Two of them are located in the centre of the larger annular construction, while the other two are outside of it (Fig. 1). Overall, about 400 pieces were used, comprising a total length of 112.4 m and an average weight of 2.2 tons of calcite (Extended Data Table 1). Half of the elements composing the structures consist of the middle part of stalagmites (that is, without the root or tip), and very few pieces are whole (~5%). The stalagmites are well calibrated with a mean length of 34.4 cm for the large (A) and 29.5 cm for the small (B) annular structures, thus strongly suggesting intentional construction (Extended Data Fig. 4). Marks left by stalagmite wrenching are seen near the structures, though in most cases the original provenance of the stalagmites is difficult to determine owing to calcite flowstones covering a large part of the cave floor.

The annular structures are composed of one to four superposed layers of aligned stalagmites (Extended Data Fig. 2b). Notably, some short elements were placed inside the superposed layers to support them (Extended Data Fig. 2d, e). Other stalagmites were placed vertically against the main structure in the manner of stays, perhaps to reinforce the constructions (Extended Data Fig. 2a–c). All of these elements, combined with the large size of the structures, exclude any interventions by bears (Supplementary Information Table 2). Although bear traces are present throughout the cave (fur, claw marks, paw prints), hibernation hollows are observed only in other sectors (End Gallery, Bear Hollow Chamber at ~80 m and 240 m from the Structure Chamber).

Traces of fire are present on all six structures (Fig. 1). They consist of 57 reddened, more or less fissured speleofacts, and 66 blackened ones (Extended Data Fig. 3). The red and black colours are clearly not related to precipitates from the dripping water since no similar traces are observed on the ceiling. Instead, most of the coloured (and

[1]PACEA, UMR 5199 CNRS-UB-MCC University of Bordeaux, 33615 Pessac, France. [2]Earth & History of Life, Royal Belgian Institute of Natural Sciences, 1000 Brussels, Belgium. [3]AMGC, Vrije Universiteit Brussel, 1050 Brussels, Belgium. [4]LSCE, UMR 8212 CNRS-CEA-UVSQ, 91400 Gif-sur-Yvette, France. [5]Société spéléologique et archéologique de Caussade, 5 rue Bourdelle 82300 Caussade, France. [6]Institute of Global Environmental Change, Xi'an Jiaotong University, Xi'an 710049, China. [7]Earth Sciences, University of Minnesota, Minneapolis, Minnesota 55455, USA. [8]Protée Expert Sas, 30250 Sommières, France. [9]Faculté Polytechnique, University of Mons, 7000-Mons, Belgium. [10]Laboratoire de Géologie de l'École Normale Supérieure de Paris (ENS), UMR CNRS 8538, 75000 Paris, France. [11]Archéosphère, 11500 Quirbajou, France. [12]Get in Situ, 1091 Bourg-en-Lavaux, Switzerland. [13]LIENSs, UMR 7266 CNRS-University of La Rochelle, 17000 La Rochelle, France. [14]Ministry of Culture, Regional Archaeological Service of Midi-Pyrénées, 31080 Toulouse, France. [15]Archéostransfert, Archéovision, UMS 3657 SHS-3D, 33007 Pessac, France.
*These authors contributed equally to this work.

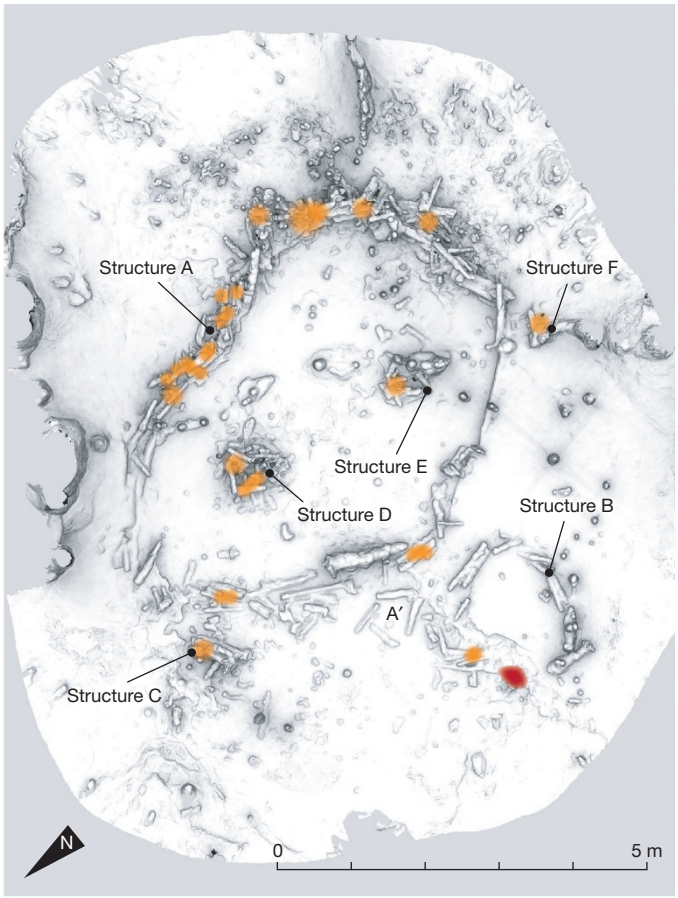

Figure 1 | Ortho-image of the Bruniquel Cave structures. The six structures are composed only of speleothems or fragments of speleothems (speleofacts), aligned and superimposed (A, B) (Extended Data Fig. 2a, b), or accumulated (C, D, E, F). A′ is a likely extension of A. Their contours are sometimes imprecise due to the calcite layer and stalagmitic regrowths that cover them. The orange spots represent the heated zones, all located on the construction elements. The red spot (structure B) represents a char concentration (mainly burnt bone fragments) on the ground (Extended Data Fig. 3, bottom left).

fissured) locations were clearly heated, as confirmed by magnetic measurements of the most visibly reddened and blackened zones (Extended Data Fig. 5). A char (that is, carbonized organic material) is located near structure B, and a dozen black fragments are observed in the structures. The largest one is a 6.7-cm-long burnt bone (diaphysis) of a bear or large herbivore found on accumulation structure E (Fig. 1). It was covered by a 6-mm-thick calcite layer that has been precisely dated (Extended Data Table 2 and Extended Data Fig. 6a, d, e). The calcite surrounding this bone is reddened, blackened and fissured. Another black fragment was trapped between the calcite regrowth and the structure (Extended Data Fig. 6b). The black fragments and bone were clearly heated, as indicated by molecular and atomic spectrometry (Extended Data Fig. 6).

The age of the constructions has been determined by uranium-series dating of the stalagmite calcite (Supplementary Information SM2): the top of stalagmites that are part of the structure give maximum ages while the bases of the stalagmite regrowths sealing the structures give minimum ages (Supplementary Information SM1).

Eighteen multi-collector ICP-MS uranium-series ages[10] with 2σ uncertainties were obtained from the calcite cores extracted from the stalagmites (Extended Data Table 2, Supplementary Information SM2).

Four additional samples were also dated: one from a core taken in the flowstone pavement inside annular structure A to evaluate its contemporaneity with the structures, and three from the calcite layer that formed on the burnt bone found inside accumulation structure E (Fig. 1).

From the five calcite regrowths covering the structure, the two oldest ages are situated in the same time window, that is, 177.9 ± 3.7 ka and 175.2 ± 0.8 ka (Fig. 2 and Extended Data Table 2). They partially cover the age of the youngest dated stalagmite in the structure (177.1 ± 1.5 ka, Extended Data Table 2). All other ages correspond with this chronology, showing that the stalagmite tips are contemporary to or older than the calcite regrowths.

These results indicate that the structure was built between 175.2 ± 0.8 ka and 177.1 ± 1.5 ka (Fig. 3). Moreover, additional evidence for human presence in the cave at this time (Extended Data Table 2; Extended Data Figs 5 and 6) is provided by the burnt bone located in structure E, older than 180.9 ± 20.3 ka, the age of the calcite that formed on its surface, and the bone fragment trapped inside the BR-stm-SB7 core, with a minimum age of 175.2 ± 0.8 ka.

The age (175.9 ± 5.7 ka) of the calcite flowstone situated inside the annular structure is similar to that of the main structure within the margin of error (176.5 ± 2.1 ka), suggesting that the climate during this period (that is, 175–177 ka), covering part of marine isotope stage 6, was sufficiently humid and warm to allow continuous calcite deposition despite generally glacial conditions (Fig. 3). It can be associated with the warm phase VI-6-5 of the nearby Villars Cave speleothem record, characterized by low $\delta^{18}O$ and $\delta^{13}C$ (ref. 11) (Extended Data Fig. 7). Other European records show a similar climatic pattern, such as the high percentage of Euro-Siberian pollen in the MD01-2444 marine core off Lisbon between ~175 and 177 ka (ref. 11).

Early Neanderthals were the only human population living in Europe during this period[12]. Our findings suggest that their society included elements of modernity, which can now be proven to have emerged earlier than previously thought. These include complex spatial organization, fire use, and deep karst occupation (Extended Data Fig. 8b).

Solid evidence for spatial organization (that is, human constructions, especially complex ones that required a social organization) during the Lower or Middle Palaeolithic is rare[13]. One hypothesis for its emergence postulates a sudden appearance of social organization with the arrival of modern humans (*Homo s. sapiens*)[14], while a second hypothesis claims a more gradual and mosaic emergence during Neanderthal times in different parts of the world, including Europe[15]. In Europe, however, completely preserved sites are exceptional before the Upper Palaeolithic (42,000 calibrated years before present)[16] and taphonomic processes hinder their identification[17,18]. The spatial organization at Bruniquel Cave is the first one attributed with certitude to the early Middle Palaeolithic. The use of stalagmites is also unique for periods older than the Upper Palaeolithic, and implies a necessary simultaneous realization of different tasks and consequently, the existence of some degree of social organization (Extended Data Fig. 8a). The location of the Bruniquel structures inside a cave, where they were protected from weathering, animals and humans, played a major role in their preservation.

The first unequivocal use of fire is dated to the Middle Pleistocene (approximately 0.8 million years ago (Ma))[19] and more than 1 Ma in southern Africa[20], with a more generalized use only after 0.3 Ma. A critical review of all known remains of fire in Europe[21] concluded that Neanderthals were the first to commonly use fire, and in particular at the end of the Middle Pleistocene when they began to cook and produce new materials such as organic glue and haft tools. During marine isotope stage 6, the average number of proven fire uses for 10,000-year time slices is 1.47, which is very low[20]. None of these sites is associated with a deep karst context.

Deep karst occupation does not appear to have occurred in Africa in any period, whether the Early or Middle Stone Age, or even the Late Stone Age if we exclude shelters and cave entrances with evidence for human presence in South Africa, Ethiopia and Maghreb (Extended

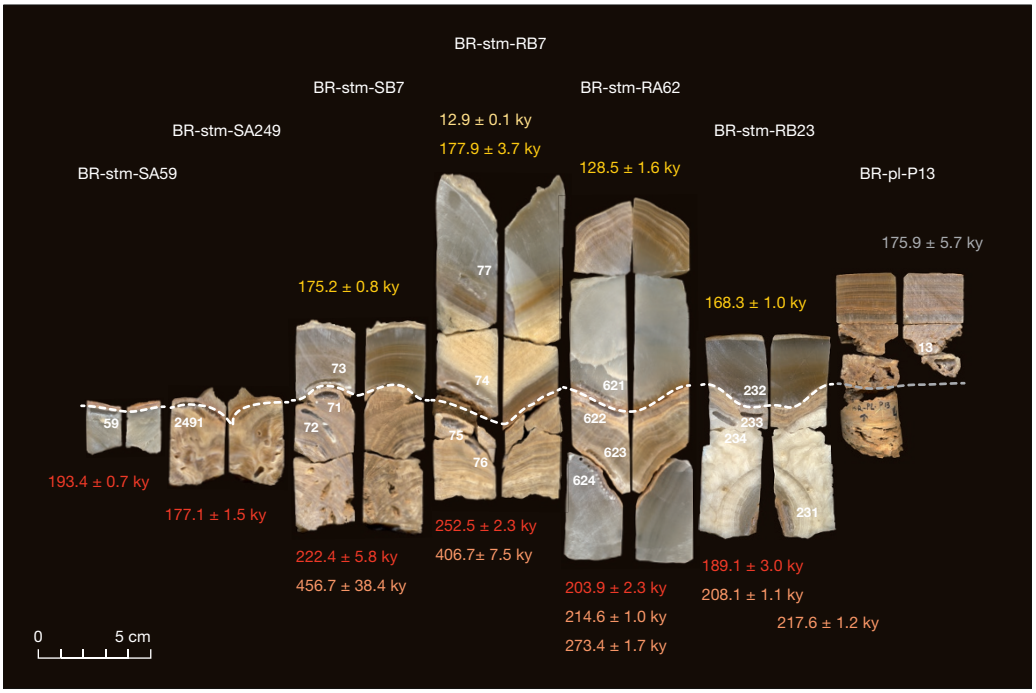

Figure 2 | The calcite cores sampled from the structures. BR-stm-SA59, BR-stm-SA249 and BR-stm-SB7 were cored from the tips of stalagmites used to build the structures. BR-stm-RB7, BR-stm-RA62 and BR-stm-RB23 were sampled at the base of stalagmites growing on the structures. All three cores display regrowth in their upper part as well as the older underlying stalagmite used as building item. Core BR-PL-P13 was taken from the flowstone located inside the main structure A. Samples were taken with a 1.6 cm (for BR-stm-SA59) and 2.6 cm diameter (for the other cores) coring device. Subsamples for uranium-series dating are indicated with their number (white). The dashed line indicates, within the deposition of calcite, the moment of the building of the structures, that is, the limit between the stalagmites used in the structure (speleofact) and the regrowths. In most cases, this limit is marked by a clay layer. The ages for samples taken under the dashed line are given below the cores (orange); the ages for samples taken above the line (yellow) are given above the cores. The ages given in red are those which give the closest maximum age for the structures. ky, thousand years. The age of the flowstone inside the structure A is given in white, since the position corresponding to the time of construction (dashed line) inside the BR-PL-P13 core is still uncertain.

Data Fig. 8). The oldest evidence for the appropriation of this difficult environment is found in Europe[22], Southeast Asia/Sunda[23], Wallacea[24] and Australia/Sahul[25]. The accumulation of human bodies by Acheuleans at Sima de los Huesos, Spain (0.35 Ma)[26] is very different from the Bruniquel structures, however. In other examples, the human frequentation of caves is linked to engraving, painting or

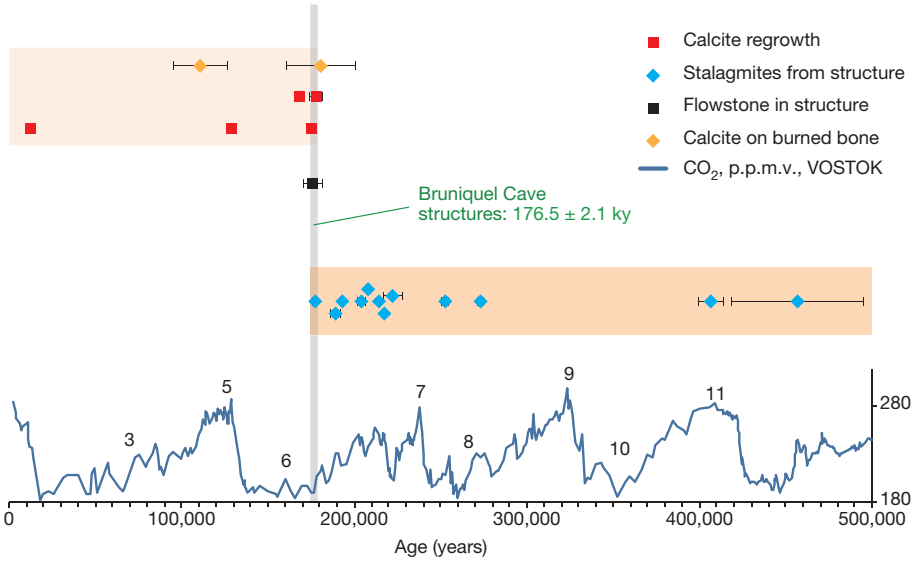

Figure 3 | Uranium-series ages (with 2σ error bars) obtained from the structures. Yellow, ages of the calcite covering the burnt bone in the accumulation structure E; red, ages obtained from the stalagmites covering the structure (regrowths) and representing a minimum age for the structure; blue, ages obtained from the stalagmites used by humans to build the structure (speleofacts) and representing a maximum age for the structures; black, age obtained from the flowstone partially covering the inside area of the main structure. The age of the structures is situated between 175.2 ± 0.8 thousand years (ky) and 177.1 ± 1.5 ky. The calcite covering the burnt bone is dated to 180.9 ± 20.3 ka, indicating a minimum age of the bone and adding evidence of earlier human presence in the cave. The general climatic context is given by the CO_2 concentration variation (expressed in p.p.m.v., low right *y* axis) extracted from the Vostok ice core record[30] (black numbers indicate major marine isotope stages).

sculpting activities. These sites are thus younger than 42,000 calibrated years before present and are always associated with *Homo s. sapiens*. Symbolic, cultural or funerary activities were the main reasons for these cave visits. Until now no evidence has been found for regular Neanderthal incursions into caves, except for a possible case of footprints[27], and Neanderthal constructions inside caves, at least at a distance that is no longer exposed to daylight, were totally unknown. Moreover, Upper Palaeolithic constructions in caves are limited to fireplaces, simple hearths, and some rock or speleothem displacements. Even in caves regularly visited since the Aurignacian, constructions are non-existent or anecdotal[28,29].

What was the function of these structures at such a great distance from the cave entrance? Why are most of the fireplaces found on the structures rather than directly on the cave floor? Based on most Upper Palaeolithic cave incursions, we could assume that they represent some kind of symbolic or ritual behaviour[3], but could they rather have served for an unknown domestic use or simply as a refuge? Future research will try to answer these questions.

The attribution of the Bruniquel constructions to early Neanderthals is unprecedented in two ways. First, it reveals the appropriation of a deep karst space (including lighting) by a pre-modern human species. Second, it concerns elaborate constructions that have never been reported before, made with hundreds of partially calibrated, broken stalagmites (speleofacts) that appear to have been deliberately moved and placed in their current locations, along with the presence of several intentionally heated zones. Our results therefore suggest that the Neanderthal group responsible for these constructions had a level of social organization that was more complex than previously thought for this hominid species.

Online Content Methods, along with any additional Extended Data display items and Source Data, are available in the online version of the paper; references unique to these sections appear only in the online paper.

Received 19 August 2015; accepted 27 April 2016.
Published online 25 May 2016.

1. Mellars, P. *The Neanderthal Legacy. An Archaeological Perspective from Western Europe,* (Princeton University Press, 1996).
2. Soressi, M. *et al.* Neandertals made the first specialized bone tools in Europe. *Proc. Natl Acad. Sci. USA* **110,** 14186–14190 (2013).
3. Soressi, M. & d'Errico, F. Pigments, gravures, parures: les comportements controversés des Néandertaliens. In *Les Néandertaliens, Biologie et Cultures* (eds Vandermeersch B. et Maureille B.) Doc. Préhist. **23,** Paris, CTHS, 297–309 (2007).
4. Maureille, B. & Vandermeersch, B. Les sépultures néandertaliennes. In *Les Néandertaliens, Biologie et Cultures* (eds Vandermeersch, B. & Maureille, B.) Doc. Préhist. 23, Paris: CTHS, 311–322 (2007).
5. Villa, P. & Roebroeks, W. Neandertal Demise: An Archaeological Analysis of the Modern Human Superiority Complex. *PLoS One* **9,** e96424 (2014).
6. Rouzaud, F., Soulier, M. & Lignereux, Y. La grotte de Bruniquel. *Spelunca* **60,** 27–34 (1996).
7. Lafon, L. *La Grotte de Bruniquel (Tarn-et-Garonne). Inventaire au Sol des Vestiges Fauniques.* Thesis, University of Toulouse Paul Sabatier (1996).
8. Lorblanchet, M. *La Naissance de l'Art. Genèse de l'Art Préhistorique* (Paris, Errance, 1999).
9. Hayden, B. Neandertal social structure? *Oxf. J. Archaeol*. **31,** 1–26 (2012).
10. Cheng, H. *et al.* Improvements in ^{230}Th dating, ^{230}Th and ^{234}U half-life values, and U-Th isotopic measurements by multi-collector inductively coupled plasma mass spectrometry. *Earth Planet. Sci. Lett.* **371–372,** 82–91 (2013).
11. Wainer, K. *et al.* Millennial climatic instability during penultimate glacial period recorded in a south-western France speleothem. *Palaeogeogr., Palaeoclim. Palaeoecology* **376,** 122–131 (2013).
12. Hublin, J.-J. The origin of Neandertals. *Proc. Natl Acad. Sci. USA* **106,** 16022–16027 (2009).
13. Otte, M. The management of space during the Paleolithic. *Quatern. Int.* **247,** 212–229 (2012).
14. McBrearty, S. & Brooks, A. S. The revolution that wasn't: a new interpretation of the origin of modern human behavior. *J. Hum. Evol.* **39,** 453–563 (2000).
15. D'Errico, F. The invisible frontier. A multiple species model for the origin of behavioral modernity. *Evol. Anthropol.* **12–4,** 188–202 (2003).
16. Tchernych, A. P. in *Molodova I: A Single Case of Mousterian Settlement in the Middle Dniestr Basin* (in Russian) (ed. Goretsky, G.I. & Ivanova, I.K.) 6–102 (Nauka, 1982).
17. de Lumley, H. *Une Cabane Acheuléenne dans la Grotte du Lazaret à Nice.* Vol. 7, Paris, Soc. Préhist. Franç. (1969).
18. Mania, D. H. *et al. Bilzingsleben II. Homo erectus – Seine Kultur und Seine Umwelt.* VEB Deutscher Verlag der Wissenschaften, Berlin (1983).
19. Goren-Inbar, N. *et al.* Evidence of hominin control of fire at Gesher Benot Ya'aqov, Israel. *Science* **304,** 725–727 (2004).
20. Berna, F. *et al.* Microstratigraphic evidence of in situ fire in the Acheulean strata of Wonderwerk Cave, Northern Cape Province, South Africa. *Proc. Natl Acad. Sci. USA* **109,** 1215–1220 (2012).
21. Roebroeks, W. & Villa, P. On the earliest evidence for habitual use of fire in Europe. *Proc. Natl Acad. Sci. USA* **108,** 5209–5214 (2011).
22. Clottes, J. *et al.* Les peintures paléolithiques de la grotte Chauvet-Pont d'Arc, à Vallon-Pont-d'Arc (Ardèche, France): datations directes et indirectes par la méthode du radiocarbon. *C.R. Acad. Sc. Paris* **320,** 1133–1140 (1995).
23. Plagnes, V. *et al.* Cross dating (Th/U-^{14}C) of calcite covering prehistoric paintings in Borneo. *Quat. Res.* **60,** 172–179 (2003).
24. Aubert, M. *et al.* Pleistocene cave art from Sulawesi, Indonesia. *Nature* **514,** 223–227 (2014).
25. Bednarik, R. The cave petroglyphs of Australia. *Aust. Aborig. Stud*. **2,** 64–68 (1990).
26. Arsuaga, J. L. Bermudez de Castro, J. M. & Carbonell, E. (Eds) The Sima de los Huesos hominid site. *J. Hum. Evol.* **33** (special issue).
27. Onac, B. P. *et al.* U-Th ages constraining the Neanderthal footprint at Vârtop Cave, Romania. *Quat. Sci.* **24,** 1151–1157 (2005).
28. Bégouën, R., Clottes, J., Feruglio, V. & Pastoors, A. *La Caverne des Trois-Frères*, Paris Somogy- Assoc. L. Bégouën (2013).
29. Delannoy, J.-J.*et al.* The social construction of caves and rockshelters: Chauvet Cave (France) and Nawarla Gabarnmang (Australia). *Antiquity* **87,** 12–29 (2013).
30. Petit, J. R. *et al.* Climate and atmospheric history of the past 420,000 years from the Vostok ice core, Antarctica. *Nature* **399,** 429–436 (1999).

Supplementary Information is available in the online version of the paper.

Acknowledgements We thank the owners of the cave (Nidauzel association), the French Ministry of Culture & Communication, MCC (DRAC-SRA Midi-Pyrénées, Toulouse), M. Vaginay, P. Chalard, É. Mauduit, the Speleological & Archaeological Society of Caussade (SSAC), CNRS (InEE & InSU), the University of Bordeaux-PACEA, LSCE Gif-s/-Yvette, M. O'Farrell and C. Garrec for editing, V. Feruglio for a drawing. We thank F. Dewilde and F. Mansouri (LSCE) for their assistance with the isotopic measurements, Y. Vanbrabant (Belgian Geological Survey) for his assistance with the cave monitoring and B. Martinez for his help with the topography. We thank S. Mariot and R. Weil (LPS, Paris-XI University, Orsay) for their help in the infrared spectrometry measurements. This work is mainly supported by French MCC (DRAC-SRA Midi-Pyrénées, Toulouse) and in part by the Belgian Science Policy Office. The U-Th dating was supported in part by the U.S. NSF.

Author Contributions J.J., S.V. and D.G. coordinated this study; they wrote the article and conducted the field sampling. M.S. participated in the cave discovery and is in charge of the logistical support and cave access. H.Ch. made the U-Th measurements and R.L.E. oversaw and helped to interpret the U/Th dates. D.B. conducted the δ^{18}O and δ^{13}C measurements. C.B. is responsible for the temperature monitoring. H.C., S.D. and X.M. realised the geographical and new topography studies of the cave. F.L.-C. realised the drawings. F.L. realised the magnetism measurements and their interpretation, D.D., D.G. and J.-N.R, the SEM-EDS, FTIR measurements and Raman spectrometry. F.M. participated in the field trips and archaeological survey. P.M. realised the photogrammetric work. C.F. realised the study of fireplaces and heated areas. É.R. participated in the field trips and the coring. F.S. is responsible for the statistical studies of the structure elements.

Author Information Reprints and permissions information is available at www.nature.com/reprints. The authors declare no competing financial interests. Readers are welcome to comment on the online version of the paper. Correspondence and requests for materials should be addressed to J.J. (jacques.jaubert@u-bordeaux.fr) or S.V. (sophie.verheyden@naturalsciences.be) or D.G. (dominique.genty@lsce.ipsl.fr).

31. Rouzaud, F., Soulier, M., Brugal, J.-Ph. & Jaubert, J. L'Igue des Rameaux (Saint-Antonin-Noble- Val, Tarn-et-Garonne). Un nouveau gisement du Pléistocène moyen. Premiers résultats. *Paléo* **2,** 89–106 (1990).
32. Faivre, J.-Ph. *et al.* In *Modalités d'Occupations et Exploitation des Milieux au Paléolithique dans le Sud-Ouest de la France: l'Exemple du Quercy* (eds Jarry, M., Brugal, J.-Ph. & Ferrier, C.), *Paléo* 4 (suppl.), 231–270 (2013).
33. Clottes, J. *et al.* In *L'Art des Cavernes. Atlas des Grottes Ornées Françaises* (Paris, Ministère de la Culture-Imprimerie Nationale), 540–551 (1984).
34. Cantalejo, P., del Mar Espejo, M., Ramos, J. & Weniger, G. C. Elementos de iluminación in *Cueva de Árdales. Intervenciones arqueológicas 2011-2014* (eds Ramos, J., Weniger, G.C., Cantalejo, P. & del Mar Espejo, M.) Ediciones Pinsapar, 119–146 (2014).
35. Brodard, A. *et al.* In *Actes du colloque MADAPCA, Micro Analyses et Datations de l'Art Préhistorique dans son Contexte Archéologique, MNHN-C2RMF, 16-18 novembre 2011*. *Paléo* (special issue) 233–235 (2014).
36. Bertran, P., Hétu, B. & Texier, J.-P. Fabric characteristics of subaerial slope deposits. *Sedimentology* **44,** 1–16 (1997).
37. Lenoble, A. & Bertran, P. Fabric of Palaeolithic levels: methods and implications for site formation processes. *J. Archaeol. Sci.* **31,** 457–469 (2004).
38. Scollar, I., Tabbagh, A., Hesse, A. & Herzog, I. *Archaeological Prospecting and Remote Sensing.* Cambridge, Cambridge University Press (1990).
39. Le Borgne, E. Influence du feu sur les propriétés magnétiques du sol et sur celles du schiste et du granite. *Ann. Geophys.* **16,** 159–195 (1960).
40. Maki, D., Homburg, J. A. & Brosowske, S. D. Thermally activated mineralogical transformations in archaeological hearths: inversion from maghemite (γFe2O3) phase to hematite (αFe2O3) form. *Archaeol. Prospect.* **13,** 207–227 (2006).
41. Carrancho, Á. & Villalaín, J. J. Different mechanisms of magnetisation recorded in experimental fires: archaeomagnetic implications. *Earth Planet. Sci. Lett.* **312,** 176–187 (2011).
42. Jrad, A. *et al.* Magnetic investigations of buried palaeohearths inside a Palaeolithic cave (Lazaret, Nice, France). *Archaeol. Prospect.* (2013).
43. Brodard, A. *et al.* Thermal characterization of ancient hearths from the cave of Les Fraux (Dordogne, France) by thermoluminescence and magnetic susceptibility measurements. *Quat. Geochronol.* **10,** 353–358 (2012).
44. Burens, A. *et al.* Benefits of an accurate 3D Documentation in Understanding the Status of the Bronze Age Heritage Cave 'Les Fraux' (France). *Int. J. of Heritage in the Digital Era* 1, 179–195 (2014).
45. Stiner, M. C. & Kuhn, S. L. Differential burning, recrystallization, and fragmentation of archaeological bone. *J. Archaeol. Sci.* **22,** 223–237 (1995).
46. Lebon, M. *et al.* Application des micro-spectrométries infrarouges et Raman à l'étude des processus diagénétiques altérant les ossements paléolithiques. *Rev. Archéométrie* **35,** 179–190 (2011).
47. Ellingham, S. T. D., Thompson, T. J. U., Islam, M. & Taylor, G. Estimating temperature exposure of burnt bone - a methodological review. *Sci. Justice* **55,** 181–188 (2015).
48. Rouzaud, J.-N., Deldicque, D., Charon, E. & Pageot, J. Carbons in the heart of energy and environment questions: a nanostructural approach. *C. R. Geosci.* **347,** 124–133 (2015).
49. Deldicque, D., Rouzaud, J.-N. & Velde, B. A Raman-HRTEM study of the carbonization of wood: a new Raman-based paleothermometer dedicated to archaeometry. *Carbon* (2016).
50. Wainer, K. *et al.* Speleothem record of the last 180 ka in Villars cave (SW France): investigation of a large delta (18)O shift between MIS6 and MIS5. *Quat. Sci. Rev.* **30,** 130–146 (2011).

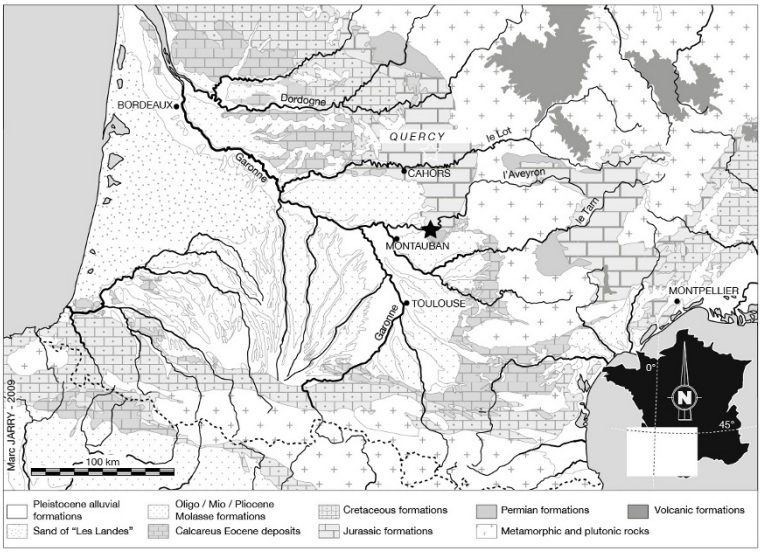

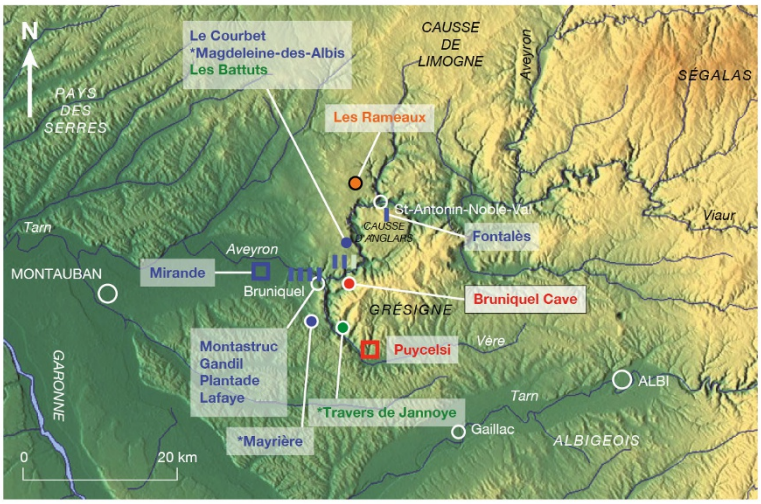

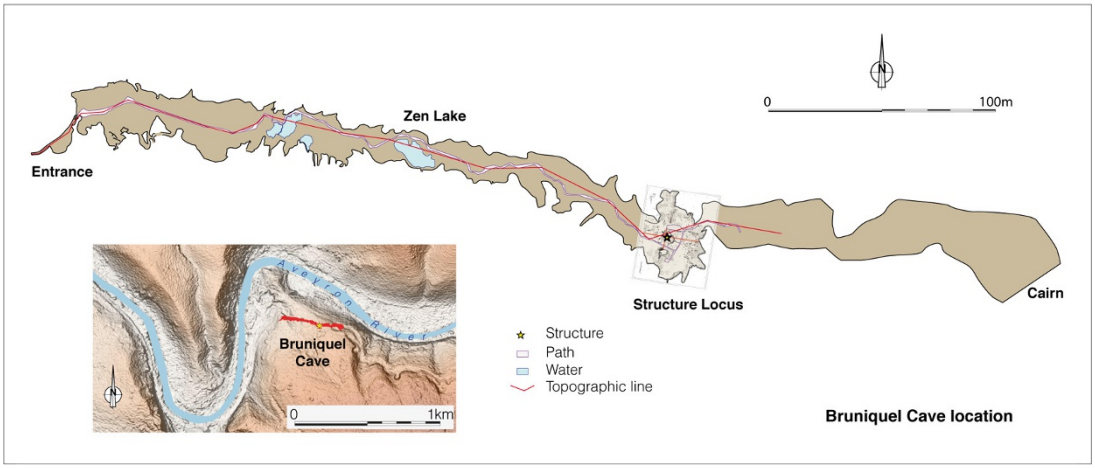

Extended Data Figure 1 | See next page for caption.

Extended Data Figure 1 | Location and map of Bruniquel Cave. **a**, Bruniquel Cave (marked with a star) is located in the southwest of France, south of the calcareous plateaus of Quercy, east of the Aquitaine Basin. Its entrance (165 m above sea level) overlooks the Aveyron valley, a tributary of the Tarn on the right bank of the Garonne and down from the Massif Central (base map courtesy of M. Jarry). **b**, Bruniquel Cave in the Aveyron valley. Orange: Lower Palaeolithic site; red: Middle Palaeolithic sites; green: early Upper Palaeolithic; blue: late Upper Palaeolithic (Magdalenian). Circles indicate caves, vertical lines indicate rock shelters and squares mark open-air sites. *Decorated caves. In this area within a 30 km zone around Bruniquel Cave, fifteen major Palaeolithic sites are known. The oldest known human occupations in this region are those of the Igue des Rameaux (Tarn-et-Garonne), a karstic sinkhole where lithic material was associated with a recent mid-Pleistocene fauna, dated from marine isotope stages 9 to 5 (ref. 31). A Middle Palaeolithic, stratified open-air site is also present at La Rouquette-Puycelsi (Tarn) upstream on the nearby Vère River[32]. The other sites are all attributable to the Upper Palaeolithic, representing the Aurignacian, Gravettian and Solutrean periods, but mainly the Magdalenian period with three decorated caves: Travers de Jannoye, La Magdeleine-des-Albis (Penne, Tarn) and Mayrière (Bruniquel, Tarn-et-Garonne)[33] (base map, courtesy of StepMap GmbH, modified by J.J.). **c**, Topography of Bruniquel Cave. The cave consists of a 10–15 m wide and 4–7 m high corridor, currently known to be 482 m long. Beyond the narrow entrance passage (filled porch), there are no major topographic difficulties until the chamber containing the structure at 336 m from the unobstructed entrance. Currently, no other access has been identified, laterally or at the other end. In this latter case, a second obstructed entrance would be at least 295 m from another slope. Sources: Structure drawn by M. Soulier and F. Rouzaud, 1992; topography realized by Protée-Expert & Get in Situ, 2015; Digital Elevation Model generated with 1957 aerial photography IGN, public domain).

f

Structures	Speleofacts		Structures A	B	C	D	E	F	Total
	Total Number		267	49	9	53	15	6	**399**
	Maximum length (m)	internal external	5.80 6.70	1.60 2.20	2.60	1.30	1.15	0.55	–
	Maximum width (m)	internal external	3.70 4.50	1.50 2.10	0.90	1.15	0.85	0.50	–
	Circumference (m)	internal external	16 20.65	5.45 7.4	0.60	4.05	3.65	1.60	**37.95**
	Surface (m^2)	internal external	16.3 23	2.3 3	0.55	1.5	1	0.3	**29.35**
	Traces of fire		12	1	1	2	1	1	**18**

Extended Data Figure 2 | Bruniquel Cave structures. a, General view of the main structure (structure A) with superposed layers of aligned stalagmites (speleofacts) Photo courtesy of É. Fabre, SSAC. **b**, Example of speleofacts accumulated over three or even four horizontal levels. **c**, Stalagmites (speleofacts) placed vertically against the main structure (structure A) in the manner of stays. **d**, **e**, Two examples of short back stalagmites serving as sustaining pieces. **f**, Summary of the metric data of the structures.

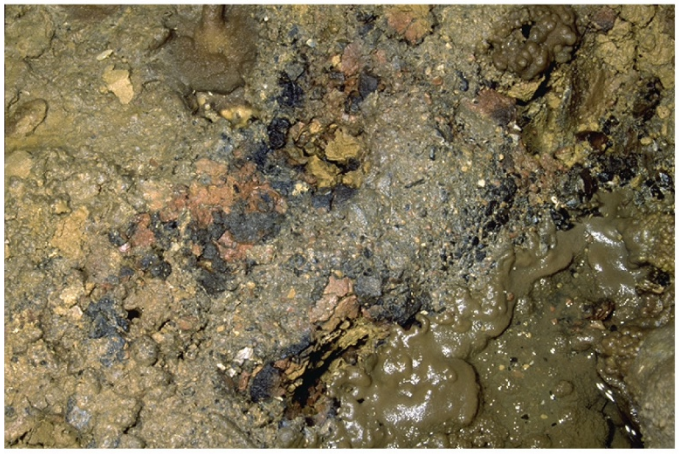

Burnt remains	Structures						Total
	A	B	C	D	E	F	
Heated areas by structure (#)	2, 3, 4, 5, 6, 7, 8, 9, 10, 11, 12, 13	1	14	15, 16	17	18	–
Total	**12**	**1**	**1**	**2**	**1**	**1**	**18**
Thermic spalling	6						**6**
Reddened spots	34	1	2	6	1	1	**45**
Reddened + Spalling	4	1		1			**6**
Total	**44**	**2**	**2**	**7**	**1**	**1**	**57**
Blackened elements/soot	46	2	4	11	3		**66**

a

b

Extended Data Figure 3 | Fireplaces and heated areas. a, Examples of a fireplace on the main structure. Note the reddened, blackened and fissured stalagmites[34]. The structure in this location (top) is covered by white, more recent and still active stalagmites. The heated areas on the speleofacts correspond to the red and grey colours, as well as fissuring and superficial spalling. These scars are similar to thermal alterations studied in the cave of Chauvet-Pont d'Arc (Ardèche)[35]. In our current stage of observation, the study of their distribution enabled us to identify a well-preserved fireplace in structure A, as well as structures that have been disturbed by processes that remain to be determined (structures D and E, for example). **b**, Numbers per structure of heated areas, thermic spalling, fissured spots and blackened elements (that is, speleofacts) and soot.

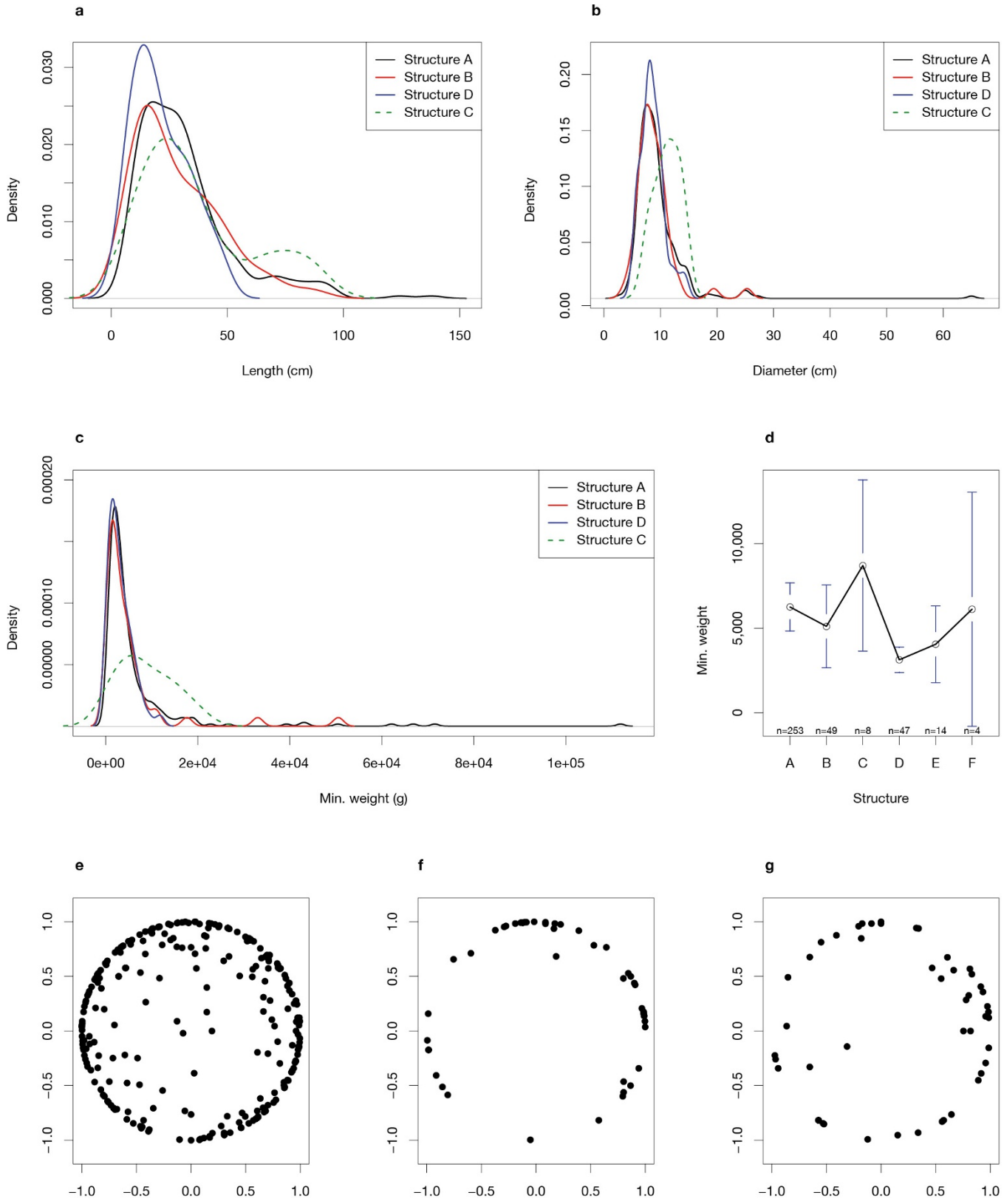

Extended Data Figure 4 | See next page for caption.

Extended Data Figure 4 | Statistics of the speleofacts. a, **b**, Kernel density estimates for the dimensions (**a**, length and **b**, diameter) of speleofacts across the different structures. Structure A can be distinguished from the others by the presence of very large speleofacts. Such speleofacts are not present in structure D, and only rarely in structure B. Structure C, despite its very small size, is worth considering due to the large dimensions of its speleofacts. Structures E and F, with only a few speleofacts and no specific features, are not represented here. A Kruskal–Wallis test conducted on the structures represented here shows a significant difference between the median length and median diameter across structures ($P < 0.05$). A post hoc analysis of the diameter with Hochberg's adjustment method, distinguishes structure C from the three others. **c**, The weight of the speleofacts is estimated by the following formula: $\pi D^2 L\rho/12 \times (1 + d/D + d^2/D^2)$ where D is the maximum diameter, d the minimum diameter, L the maximal length, and ρ the calcite density. These weights can be roughly estimated by considering them as truncated cones. As their maximum length L, maximum diameter D, and minimum diameter d are known, their volume can be easily estimated (Extended Data Table 1). Their weight is then obtained by multiplying the previous quantity by the calcite density ρ, which is comprised between 2.5 and 2.8 $g\,cm^{-3}$ depending on its porosity and detrital contamination. Minimal weights are obtained using a density of 2.5 $g\,cm^{-3}$. **d**, The figure shows the mean weights and their 95% confidence interval in each structure. **e**–**g**, The orientation data (Schmidt diagram[36]) of the speleofacts in the three main structures (A, B, D) are very similar (**e**, structure A; **f**, structure B; **g**, structure D) and do not show any preferential direction. The distance to the centre of the circle represents the slope; the distribution of the speleofacts is isotropic and mostly planar. This confirms in all cases that such orientation and slope patterns cannot be due to natural processes related to water flow, mass flows or other gravitational processes[37], which in any case would not have resulted in the current geomorphology of the cave in this sector.

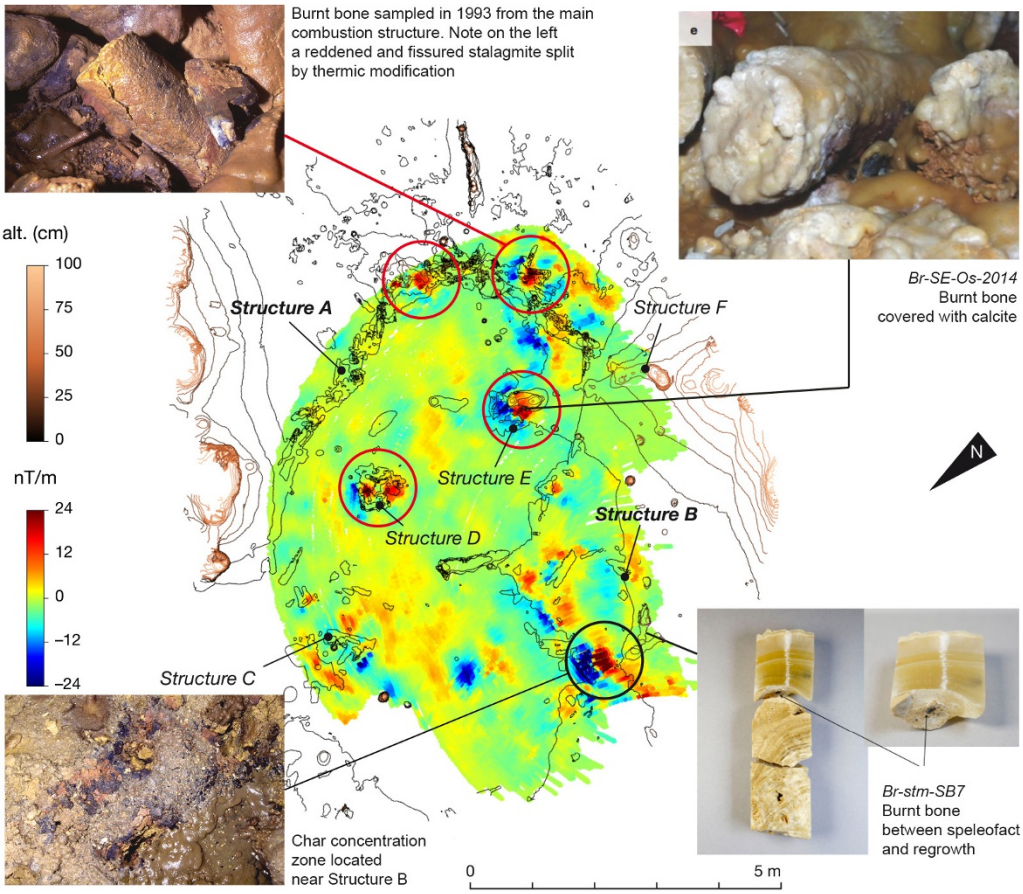

Extended Data Figure 5 | Magnetic survey above the structures. Red circles: main recognized hearths. The magnetic survey aims to reveal the locations that were heated, including hearths or smaller fireplaces through the detection of magnetic anomalies. The first archaeological applications of this prospection method are for the location of heated archaeological structures (see pages 422–519 of ref. 38). The magnetic properties enhancement by heating was first demonstrated for soils[39–41], and then on substrate of caves[42–44]. In this type of hydromorphic environment, iron is present as nonmagnetic or weak magnetic FeOOH minerals, such as goethite (see pages 375–421 of ref. 38). In these conditions, temperature elevation above 200–250 °C induces dehydration of the FeOOH, present in clay material, to Fe_3O_4 (magnetite) which is a strong magnetic mineral[43]. The increase of magnetic susceptibility induced by heating offers similar information than thermoluminescence methods[43]. In the present case, a magnetic susceptibility increase beyond a factor of two was observed after heating a clay sample of the cave. Therefore, the heated clay-like material, even if present only in small amounts in speleothems, acquired a sufficiently high magnetization to generate a local earth magnetic deformation, also called an anomaly. As this deformation decreases when the source distance increases (see pages 422–519 of ref. 38), a larger anomaly with a medium intensity might reveal a hearth under the stalagmitic floor (between structures B and C), calcite being magnetically nearly neutral (diamagnetic). The realization of magnetic survey at high spatial resolution for detection of paleohearths in prehistoric cave is a recent innovation[44]. The magnetic field explored above the structures was over one metre thick, with a dual sensor G858 Geometrics magnetometer with an extended cable. A 360° prism was inserted between both sensors, which were superposed at a distance of 0.22 m. These elements were hung at the end of a telescopic boom pole and fixed on a tripod. 3D geolocation measurements were ensured by tracking with a Trimble S8 total station following the 360° prism. This apparatus allows coverage of a volumetric space up to 5 m from the operator with ten measurements per second while controlling the space covered[44]. Extended Data Fig. 5 presents the results of the magnetic measurements. Altitude contour lines (8.5 cm distance interval) are extracted from photogrammetric data. The magnetic intensity point cloud is a bottom view of the magnetic field intensity gradient, that is, the difference in magnetic field intensity as measured between the bottom and top sensors. As the local past and present magnetic field have an inclination of ~63° down, a magnetic source generates a dipolar local deformation of the magnetic field with a negative anomaly to the north and positive to the south[38]. In Extended Data Fig. 5, a dipole corresponds to a blue and red spot aligned approximately north–south. The majority of the main dipoles of metric dimension observable are mostly associated to fire traces (reddened, blackened calcite) observed on the horizontally positioned stalagmites, for example, the heated zone of the structures D and E. Increases of magnetic viscosity, known as a fire marker[42], are observed in such zones. Some places present split positive anomalies, for example, places located on structure D, indicating twin core fires or non-contemporaneous fires. The main measured dipole is located to the west of structure B at the border of a zone covered by a calcite layer and near a char concentration zone, which suggests the occurrence of a hearth underneath the flowstone. Some visible heated zones did not reveal any magnetic anomaly, indicating that the substratum at these places was heated below 200–250 °C. The most tenuous dipoles located on the flat ground surface may reflect the changing nature of the substratum, rather than any heating. Indeed, the weak magnetic contrast between clay material and calcite material can be the source of a weak anomaly. An alternative explanation is the presence of a heated zone underneath a thick stalagmitic floor, the distance between source and measurement mitigating the anomaly[38]. For example, an anomaly located at midway between structures B and C. Complementary analysis of the spatial distribution of the clay material must be realized to determine which hypothesis is correct.

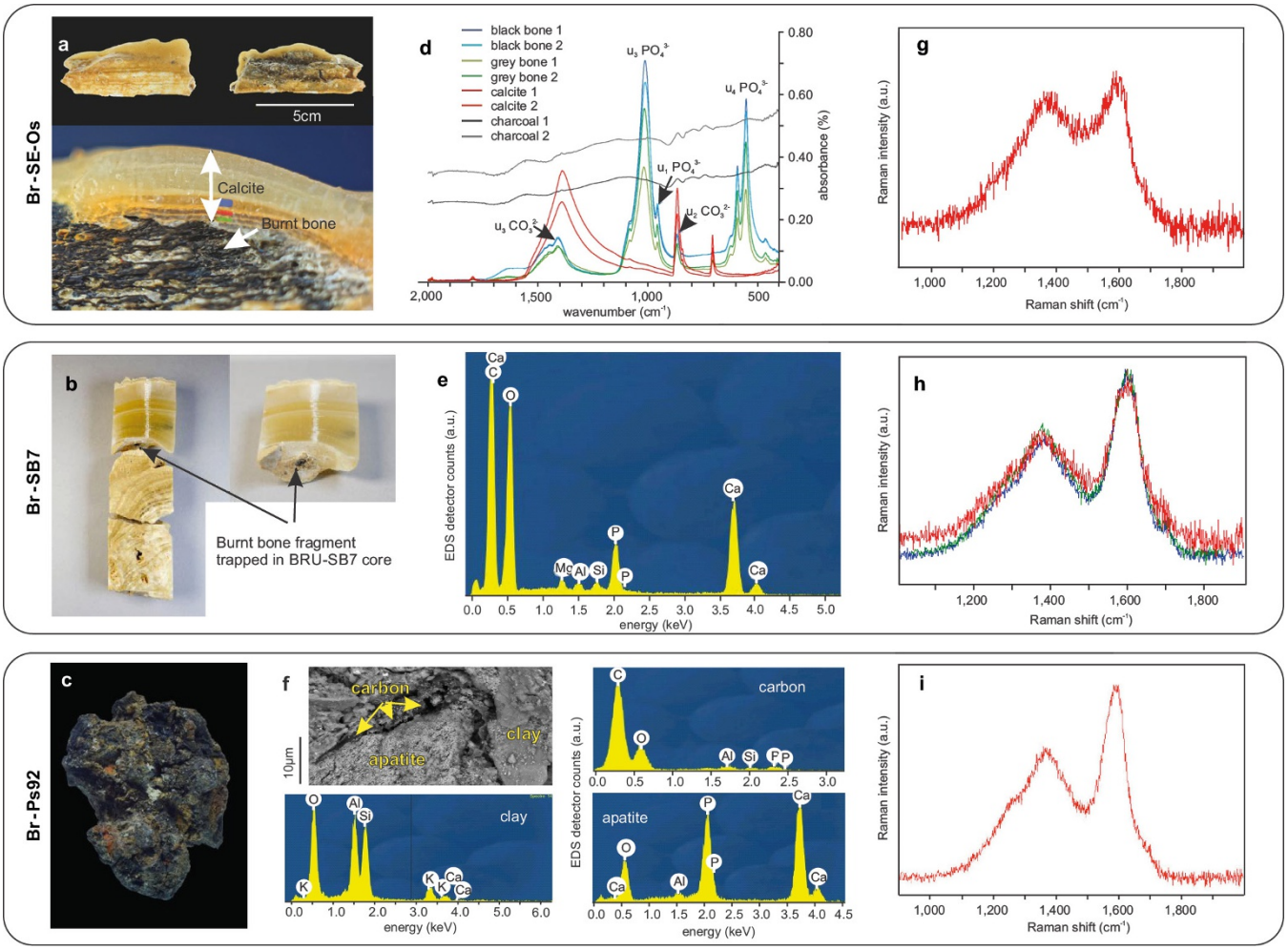

Extended Data Figure 6 | Burnt bone fragments. Three black fragments (**a**, **b**, **c**) were analysed with a scanning electron microscope energy dispersive spectrometry probe (SEM–EDS) (**e**, **f**), fast Fourier infra-red, FTIR (**d**) and Raman spectrometry (**g**, **h**, **i**). FTIR analyses were made at the Laboratoire de Physique des Solides (LPS), Paris-XI University, Orsay by S. Mariot on a Nicolet iS50 ABX spectrometer. Raman spectroscopy was performed with an Invia spectrometer from Renishaw and the atomic spectrometry was performed with a FE-SEM Zeiss Sigma equipped with an EDS probe at the École Normale Supérieure, Paris, France. **a**, A 6.7-cm-long piece of burnt bone (Br-SE-Os) trapped between stalagmite elements in structure E (Extended Data Fig. 5) was almost completely covered by calcite except on its medullar side. Three layers were sampled for uranium-series dating (green, red and blue marks) (Extended Data Table 2). The bone with the 5-mm-thick calcite crust was cut longitudinally and the calcite was sampled along deposition layers, starting at the internal surface after removing the bone material. Three thin discontinuities marked by thin brownish layers separate the deposits into three calcite layers from which three ^{230}Th samples were taken (Extended Data Table 2). Except the middle sub-sample, which was contaminated by detrital elements (high ^{232}Th concentration), ^{230}Th ages given by the other two sub-samples are in stratigraphic order and in agreement with the age of the structures. This demonstrates that humans introduced this bone before 180.9 ± 20.3 ka. Note the elongated medulla cells of the bone and their deep black colour, suggesting that the collagen was carbonized at a temperature between 300 and 400 °C[45,46]. Note that the burnt bone was covered by a reddish and blackened speleofact (Extended Data Fig. 5), due to the heat. **d**, FTIR spectroscopy (blue spectrum on the black part of the bone, green spectrum on the grey part of the bone, red spectrum on the overlying calcite crust and grey spectrum on a modern char) show well-characterized PO_4^{3-} absorbance peaks, suggesting that the bone was burnt; such as the slightly more individualized peak at ~618 cm^{-1}; and the splitting factor (SF) calculated with the heights of the 603 and 565 cm^{-1} peaks, which are here relatively high (4.6 to 4.8) and typical of burnt bones[47]. **g**, Raman spectrometry displays two well-defined peaks at 1,580 cm^{-1} and at 1,350 cm^{-1}, characteristic of char, demonstrating that it was burnt[48,49]. **b**, Sample Br-SB7 is a 3 mm large black fragment found trapped in the core of Br-stm-SB7 (Fig. 2). This fragment is situated just below the base of the regrowth dated to 175.2 ± 0.8 ka, and just above the ancient surface of the 'old' stalagmite (whose layers have been dated to 222.4 ± 5.8 ka). **h**, Raman spectra of this black fragment display two well-defined peaks at 1,580 cm^{-1} and at 1,350 cm^{-1} characteristic of char carbon[49,50]. **e**, SEM–EDS shows the presence of phosphorous, in addition to carbon, suggesting that it is a burnt bone fragment, similar to the larger bone piece (**a**). Because it is trapped in the dated calcite core, it also demonstrates that the fire occurred before 175.2 ± 0.8 ka. **c**, A black aggregate of millimetre-sized fragments (Br-PS92), mainly burnt bones of 1–3 cm was collected in 1992 by F. Rouzaud in the char concentration zone near structure B (Extended Data Fig. 5), and analysed recently. **i**, As with the previous samples, the Raman spectrum is typical of char carbon with vibrational bands at 1,580 cm^{-1} and 1,350 cm^{-1}. **f**, The SEM images (back scattered mode) show a blend of at least three phases at the micrometre scale. The elemental analyses performed by EDS on each of these phases allow their attribution to a carbonaceous component (the EDS spectrum shows a major peak of carbon), a phosphorous component (the three major peaks (Ca, P and O) strongly suggest a phase belonging to the apatite family), and a clay component (attested by the coexistence of the three major peaks Si, Al, O), respectively. The Raman spectra demonstrate that the carbonaceous component is a char[48,49], that is, a carbonaceous solid resulting from the heat treatment of an organic precursor. These results confirm that the char concentration zone near structure B was most probably a hearth, and that humans burned bones on the clay-like soil of the cave.

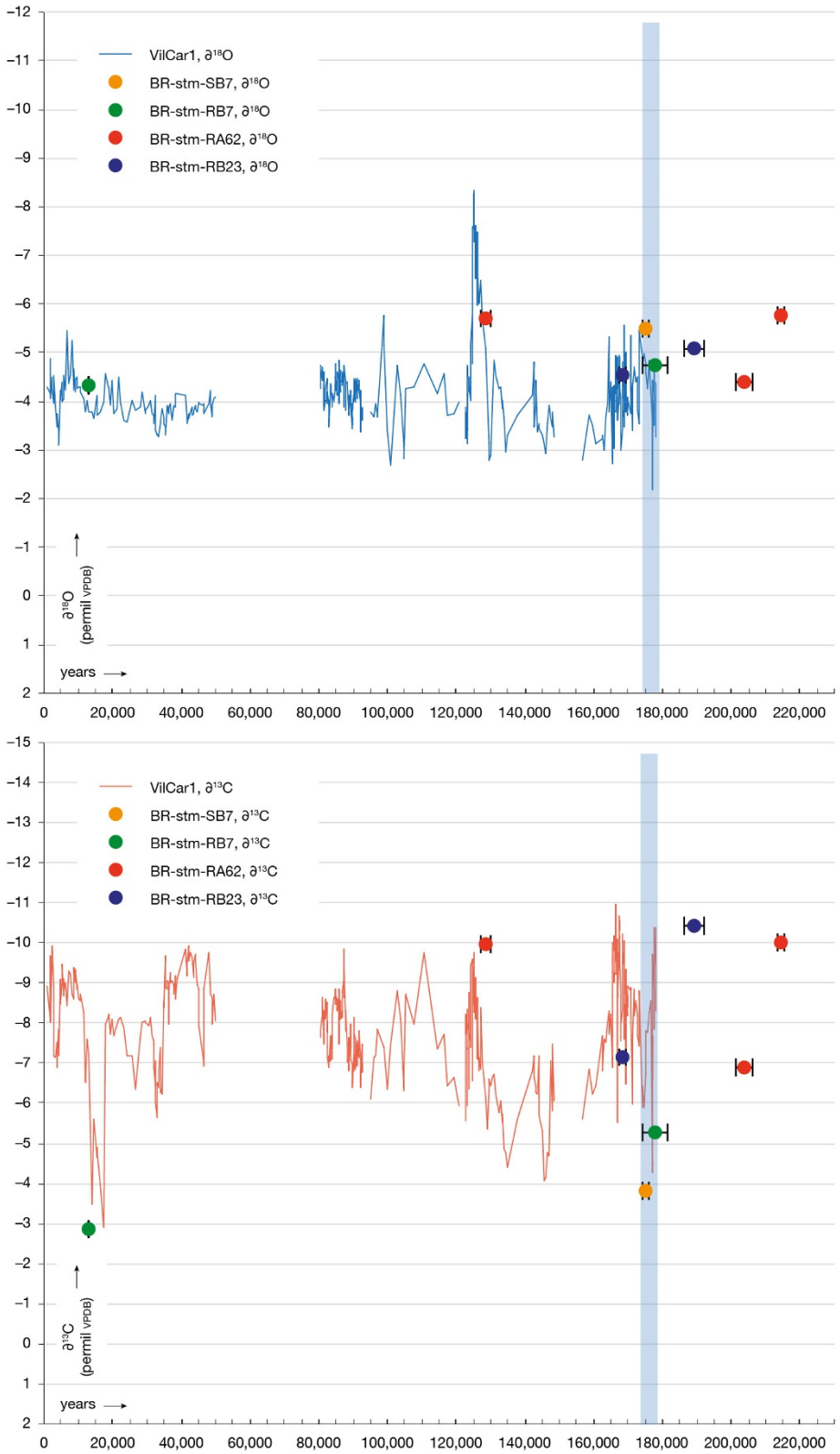

Extended Data Figure 7 | Calcite core stable isotope results. a, **b**, Stable isotope measurements (calcite $\delta^{18}O$ and $\delta^{13}C$) were made on parts of cores extracted from the structure to check the coherency of the isotope signal with an already published time series from speleothems from the Villars Cave (Dordogne)[50], located 100 km to the northwest of Bruniquel Cave. The results reveal a good match between the average $\delta^{18}O$ of regrowths after 176 ka and the Vil-car1 flowstone stable isotopes. This is also true for the sample that covers marine isotope stage 5e, with a much lower amplitude change, however. The Bruniquel core $\delta^{13}C$ signal appears more variable, possibly due to a greater sensitivity of the vegetation density to climatic changes or to detrital contaminations, which are probably close to the discontinuity at the base of the regrowths (**b**). Higher resolution measurements combined with more uranium-series dating will allow the construction of short palaeoclimatic time series and more detailed observations of climatic variations. Today, the Structure Chamber has an extremely stable temperature of 12.68 ± 0.02 °C (two times the standard deviation of the temperature values measured during one year with a time step of 1.5 h) compared to the outside temperature over the same period (13.2 ± 8.8 °C). These results indicate the current confinement of the cave environment, important for isotopic studies.

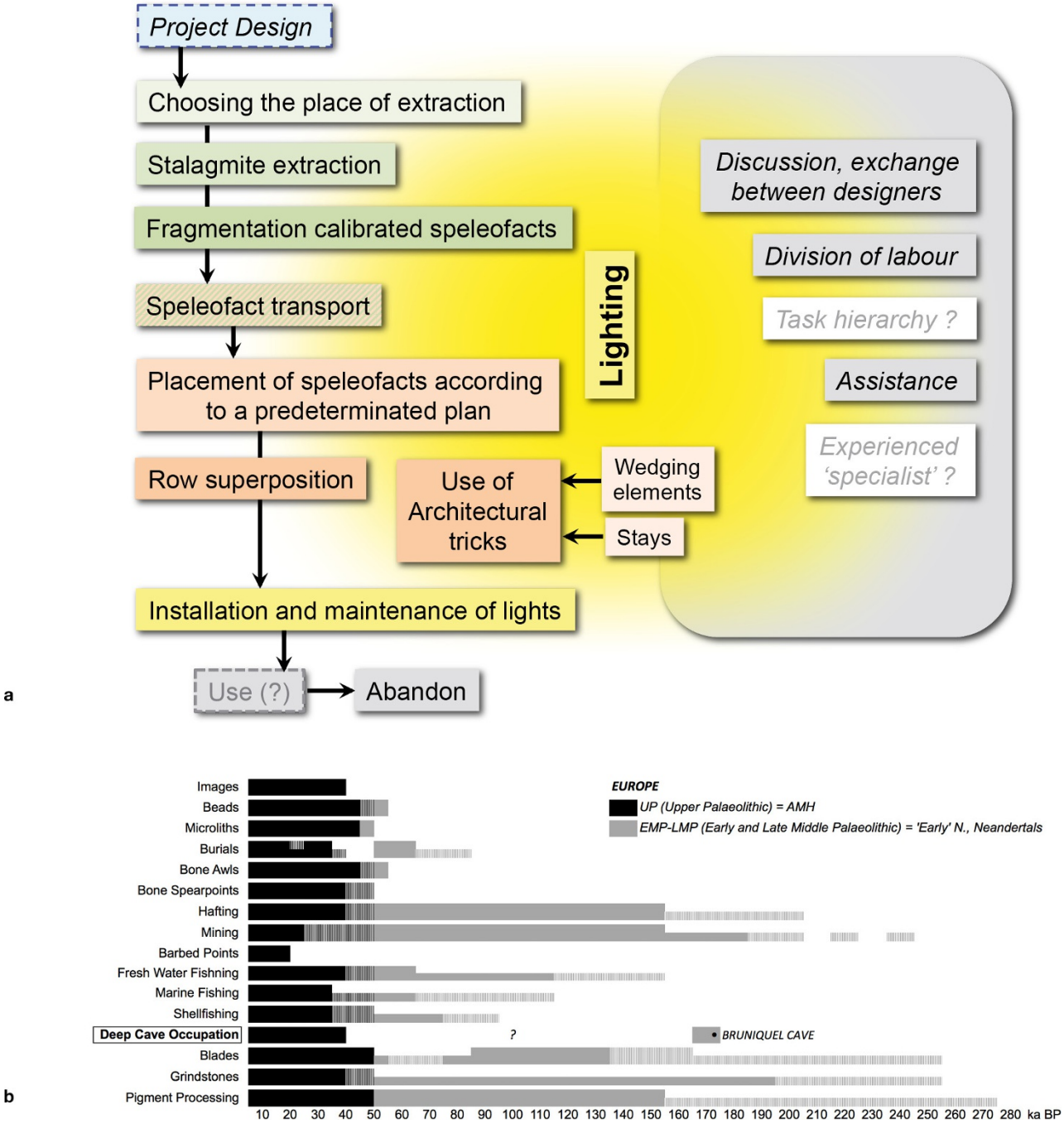

Extended Data Figure 8 | Human appropriation of the underground environment: above, the specific task sequence in Bruniquel Cave (**a**). Below, replacement within the general context of various indicators of modern behaviour (**b**). **a**, *Chaîne opératoire* (task sequence) of the construction of the structures in Bruniquel Cave. This type of construction implies the beginnings of a social organization: this organization could consist of a project that was designed and discussed by one or several individuals, a distribution of the tasks of choosing, collecting and calibrating the speleofacts, followed by their transport (or vice versa) and placement according to a predetermined plan. This work would also require adequate lighting. The construction of such a structure, involving the placement and arrangement of speleofacts, supposes a minimum degree of skill, since architectural techniques such as inserting wedging elements between two rows of speleofacts (Extended Data Fig. 2d, e), or placing stays to act as a buttresses (Extended Data Fig. 2c), appear to have been used. We evaluated the number of speleofacts used (approximately 400), as well as their combined weight (between 2.1 and 2.4 tons), but not yet the number of hours necessary to realize the structures. This will require long and complex experimental procedures that will be undertaken in future research. The complexity of the structure, combined with its difficult access (335 m from the cave entrance), are signs of a collective project and therefore suggest the existence of an organized society that was already on the path to 'modernity'. Until now, no site of this age, attributed to Neanderthals—even late ones—or early modern humans has been associated with such activities in an underground space. **b**, A multiple species model for the origin of behavioural modernity in Europe. Modified from ref. 15, to which was added the 'Deep Cave Occupation' and 'Bruniquel Cave'.

Extended Data Table 1 | Speleofacts: definition and archaeometry

Speleofacts			Structures						Total
			A	B	C	D	E	F	
Number	Number of speleofacts		267	49	9	53	15	6	**399**
	% / total		*66.92%*	*12.28%*	*2.26%*	*13.28%*	*3.76%*	*1.50%*	*100*
Length (m)	Total length of the speleofacts (m)		83.74	13.95	3.28	11.17	4.14	1.40	**117.68**
	% / total		*71.16%*	*11.85%*	*2.79%*	*9.50%*	*3.52%*	*1.19%*	*100*
	Average length		31.7	28.5	36.4	21.5	27.6	23.3	**29.8**
Weight (kg)	Weight (kg)	high estimate	1,771.28	280.28	77.97	164.65	63.45	27.42	**2,385.04**
		low estimate	1,581.50	250.27	69.62	147.01	56.65	24.48	**2,129.52**
	% / total		*74.27%*	*11.75%*	*3.27%*	*6.90%*	*2.66%*	*1.15%*	*100*
	Average weight		6,251	5,107.5	8,702.4	3,127.8	4,046.3	6120	
Diameter Ø (cm)	Ø "root" (extraction)		16.50	15.48	28.50	13.94	16.50	–	
	maximum Ø		9.41	8.91	11.17	8.54	7.95	9.33	
	minimum Ø		7.17	7.16	9.02	7.14	6.80	8.87	

A speleofact is defined as any element extracted from a speleothem (stalagmite, stalactite, drapery, flowstone, stalagmitic column, etc.) with the intent to use it for a precise purpose, thus removing it from its original formation location. This use is linked to a human activity, such as in the realization of any type of modification or construction, use as a utensil or for decoration, or for any other purpose. From the moment it is collected, the element in question attains a status that is distinct from its natural formation context, whether or not it is transformed by flaking, shaping, retouching, striking, engraving, painting, etc. Speleothems that have been clearly worked (flaked, shaped, retouched, pecked, engraved, painted, etc.) while remaining *in situ* should also be included in this definition.

Extended Data Table 2 | Speleothem ^{230}Th dating results

Core Number	Sample Number	^{238}U (ppb)	^{232}Th (ppt)	^{230}Th / ^{232}Th (atomic × 10^{-6})	δ^{234}U* (measured)	^{230}Th / ^{238}U (activity)	^{230}Th Age (ky) (uncorrected)	^{230}Th Age (ky) (corrected)	$\delta^{234}U_{initial}$ ** (corrected)	**^{230}Th Age (ky BP)*** (corrected)**
Speleothems in the structures ('speleofacts')										
BR-stm-SA249	2491	205.4 ± 0.3	16,704 ± 335	256 ± 5	466.2 ± 2.4	1.2620 ± 0.0028	178.5 ± 1.2	177.1 ± 1.5	769 ± 5	**177.1 ± 1.5**
BR-stm-RA62	621	90.5 ± 0.1	14,623 ± 293	146 ± 3	898.7 ± 2.8	1.4299 ± 0.0032	130.6 ± 0.6	128.6 ± 1.6	1,292 ± 7	**128.5 ± 1.6**
BR-stm-RA62	622	154.9 ± 0.2	30,279 ± 607	125 ± 3	593.6 ± 2.3	1.4766 ± 0.0027	206.8 ± 1.3	204.0 ± 2.3	1,056 ± 8	**203.9 ± 2.3**
BR-stm-RA62	623	133.4 ± 0.1	4037 ± 81	811 ± 16	583.5 ± 1.4	1.4885 ± 0.0019	215.0 ± 0.9	214.6 ± 1.0	1,069 ± 4	**214.6 ± 1.0**
BR-stm-RA62	624	98.9 ± 0.1	1131 ± 23	2,309 ± 46	573.1 ± 1.7	1.6008 ± 0.0019	273.6 ± 1.7	273.5 ± 1.7	1,240 ± 7	**273.4 ± 1.7**
BR-stm-SB7	71	330.8 ± 0.8	150,823 ± 3,036	50 ± 1	462.0 ± 3.3	1.3907 ± 0.0044	229.8 ± 2.7	222.5 ± 5.8	866 ± 15	**222.4 ± 5.8**
BR-stm-SB7	72	134.8 ± 0.2	242,876 ± 4,870	13 ± 1	306.0 ± 2.5	1.4098 ± 0.0086	484.4 ± 40.1	456.8 ± 38.4	1,111 ± 122	**456.7 ± 38.4**
BR-stm-SB7	73	68.2 ± 0.1	1,939 ± 39	809 ± 16	612.9 ± 1.7	1.3954 ± 0.0021	175.7 ± 0.7	175.3 ± 0.8	1,005 ± 4	**175.2 ± 0.8**
BR-stm-RB7	74	95.1 ± 0.1	30,522 ± 611	70 ± 1	548.3 ± 1.8	1.3574 ± 0.0028	183.0 ± 1.0	178.0 ± 3.7	906 ± 10	**177.9 ± 3.7**
BR-stm-RB7	75	246.2 ± 0.3	31,548 ± 632	176 ± 4	401.9 ± 1.9	1.3684 ± 0.0019	254.6 ± 1.8	252.5 ± 2.3	820 ± 7	**252.5 ± 2.3**
BR-stm-RB7	76	219 ± 0.2	45,447 ± 910	106 ± 2	267.5 ± 1.6	1.3345 ± 0.0020	410.1 ± 7.3	406.8 ± 7.5	843 ± 18	**406.7 ± 7.5**
BR-stm-RB7	77	133 ± 0.2	9 ± 1	48,099 ± 2,907	801.2 ± 1.8	0.2040 ± 0.0012	13.0 ± 0.1	13.0 ± 0.1	831	**12.9 ± 0.1**
BR-stm-SA59	59	224.8 ± 0.2	744 ± 15	8,828 ± 178	922.1 ± 1.8	1.7723 ± 0.0020	193.5 ± 0.7	193.4 ± 0.7	1,592 ± 4	**193.4 ± 0.7**
BR-stm-RB23	231	92.5 ± 0.1	1,595 ± 32	1241 ± 25	401.6 ± 1.7	1.2991 ± 0.0017	217.9 ± 1.2	217.7 ± 1.2	742 ± 4	**217.6 ± 1.2**
BR-stm-RB23	232	87 ± 0.1	4,889 ± 98	421 ± 8	688.1 ± 2.1	1.4422 ± 0.0026	169.1 ± 0.8	168.3 ± 1.0	1,106 ± 5	**168.3 ± 1.0**
BR-stm-RB23	233	147 ± 0.2	34,055 ± 683	91 ± 2	433.6 ± 1.7	1.2724 ± 0.0022	193.1 ± 1.0	189.2 ± 3.0	740 ± 7	**189.1 ± 3.0**
BR-stm-RB23	234	76 ± 0.1	157 ± 3	10,295 ± 209	409.7 ± 1.6	1.2859 ± 0.0019	208.2 ± 1.1	208.2 ± 1.1	737 ± 4	**208.1 ± 1.1**
Flowstone inside Structure A										
BR-PL-P13	13	163.2 ± 0.2	82,660 ± 1,655	45 ± 1	564.0 ± 1.8	1.3757 ± 0.0034	183.8 ± 1.2	175.9 ± 5.7	927 ± 15	**175.9 ± 5.7**
Stalagmites on the collapsed rocks in the entrance zone										
BR-stm-3	31	41.8 ± 0.1	2,780 ± 56	226 ± 5	203.2 ± 1.5	0.9104 ± 0.0020	144.5 ± 0.8	143.0 ± 1.3	304 ± 3	**142.9 ± 1.3**
BR-stm-3	32	15.7 ± 0.1	14,278 ± 286	17 ± 1	139.1 ± 3.7	0.9476 ± 0.0080	181.2 ± 4.1	157.1 ± 17.9	217 ± 12	**157.0 ± 17.9**
BR-stm-2	21	32.5 ± 0.1	21,647 ± 434	25 ± 1	131.7 ± 2.8	0.9959 ± 0.0050	211.0 ± 3.6	194.0 ± 12.6	228 ± 9	**193.9 ± 12.6**
BR-stm-2	22	28.1 ± 0.1	13,737 ± 275	34 ± 1	143.0 ± 2.6	0.9975 ± 0.0035	204.9 ± 2.5	192.9 ± 8.9	246 ± 8	**192.8 ± 8.9**
Flowstone on the collapsed rocks at the beginning of the main gallery										
BR-PL-1	1	68.5 ± 0.1	4,066 ± 81	316 ± 6	132.9 ± 1.4	1.1389 ± 0.0017	367.4 ± 5.8	366.1 ± 5.8	373 ± 7	**366.0 ± 5.8**
Calcite on the burnt bone										
Calos	Calos-1	136 ± 0.1	210,059 ± 4,206	15 ± 0	497.7 ± 1.9	1.3792 ± 0.0045	208.2 ± 1.9	180.9 ± 20.3	829 ± 48	**180.9 ± 20.3**
Calos	Calos-2	117 ± 0.2	500,389 ± 10,028	6 ± 0	467.3 ± 2.0	1.5061 ± 0.0102	296.3 ± 8.4	198.6 ± 9.5 × 10^{21}	818 ± 504	**198.5 ± 9.5 × 10^{21}**
Calos	Calos-3	50 ± 0.1	55,973 ± 1,122	16 ± 0	463.7 ± 2.4	1.0834 ± 0.0044	132.3 ± 1.1	110.6 ± 15.8	634 ± 28	**110.6 ± 15.8**

The table shows the dating of stalagmites used to build the structures (speleofacts), those of the stalagmites that grew on the structures (regrowths, in darker lines), the flowstone inside the main structure A, and the calcite on the entrance collapse. The dating results of the calcite, deposited on the burnt bone found in the structures, are shown in the last lines. One date was rejected (Calos-2) due to its high uncertainty. Corrected ^{230}Th ages assume the initial ^{230}Th/^{232}Th atomic ratio of $4.4 \pm 2.2 \times 10^{-6}$, which is the value for a material at secular equilibrium, with the bulk earth ^{232}Th/^{238}U value of 3.8. Errors are arbitrarily assumed to be 50%. Age uncertainties are given as 2σ.
p.p.b., parts per billion, 1×10^{-9}; p.p.t., parts per trillion, 1×10^{-12}; BP, before present, with the present defined as 1950 AD.